2015-1664

Experiments on Fairing Design for a Wind Turbine Tower

Kyle O'Connor*, Eric Loth†
University of Virginia, Charlottesville, VA, 22904

Michael S. Selig‡
University of Illinois at Urbana-Champaign, Urbana, IL, 61801

An aerodynamic fairing can reduce the effects of the wind turbine tower wake on the blades of a downwind rotor. Previous studies on fairing design have focused on idealized conditions and time-averaged drag reductions, whereas this is the first study to obtain and analyze unsteady velocity field data in the wake of minimum drag fairings at non-zero angles of attack, specifically designed for wind turbine towers. Experiments were conducted in a water channel using flow visualization and PIV to analyze the effect of the fairing on the tower wake compared to a typical cylindrical tower. The two tested fairing geometries, a C30u and an E863 airfoil, resulted in significant reduction of the wake deficit when the airfoils were aligned with the incoming flow. At an angle of attack of 10°, the airfoils produced wake deficits comparable to the cylinder wake, although the performance of the airfoils was improved farther downstream. Due to the self-aligning nature of the fairing, it should not be misaligned with the incoming flow direction for an extended period of time. Furthermore, the flow is more likely to remain attached at the full-scale Reynolds number, which would lead to further improvement in the performance of the fairing. Both of the fairing designs that were tested could be used to significantly reduce the effects of a cylindrical tower wake on a downwind rotor if the yaw angles can be held to less than 10°.

Nomenclature

α	=	angle of attack
α_c	=	corrected angle of attack
c	=	chord length
$C_{l,u}$	=	uncorrected 2-D lift coefficient
$C_{m,c/4,u}$	=	uncorrected 2-D moment coefficient about the quarter chord
D	=	tower/inscribed cylinder diameter
h	=	test section height
Re_D	=	Reynolds number based on tower diameter
σ	=	standard deviation, tunnel correction parameter
u	=	flow velocity in the x-direction
v	=	flow velocity in the y-direction
X	=	horizontal distance from the left edge of the interrogation window (positive to the right)
Y	=	vertical distance from the top edge of the interrogation window (positive upwards)

I. Introduction

A. Potential Benefits and Drawbacks for Downwind Turbines

The rated power for wind turbines is increasing constantly, with present large-scale systems around 5-10 MW. Future extreme-scale (10+ MW) systems will be difficult to construct using conventional rotor designs due to the combination of the blade stiffness constraints and increases in blade mass. The rotor cost is directly proportional to the mass, and the rotor accounts for a significant amount of the total system cost, with many other turbine components increasing in scale and cost as the rotor mass increases. Thus, new concepts in wind turbine design are needed to make extreme-scale wind turbines cost effective.

Conventional upwind turbine configurations typically employ blades with fiberglass shells to carry the structural and aerodynamic loads with high stiffness, in order to minimize aeroelastic deflection to avoid tower

* Graduate Researcher, Mechanical and Aerospace Engineering, 122 Engineer's Way, AIAA Member
† Professor, Mechanical and Aerospace Engineering, 122 Engineer's Way, AIAA Associate Fellow
‡ Associate Professor, Aerospace Engineering, 104 S. Wright St., AIAA Senior Member

strikes and structural fatigue. This blade stiffness needed to avoid tower strikes and fatigue leads to the aforementioned blade mass problems. This stiffness constraint can be relaxed if a downwind rotor concept is employed. In particular, recent studies[1-2] have indicated that downwind designs can thus reduce overall rotor mass for systems of 10 MW or more. For example, a segmented ultralight morphing rotor (SUMR) design allows the rotor to morph as the wind speeds increase and fully-align with the resultant forces at higher wind speeds. By allowing the forces to align along the blade, the structural loads are reduced to primarily acting in tension, which significantly reduces the cantilever loads on the blades. The downstream angle needed for alignment increases with turbine rated power, making the morphing concept more important for larger systems. Initial tests showed that this force-aligned design may allow for a substantial reduction in blade mass compared with a conventional blade.[1] Even moderate sized turbines may benefit from downwind designs. For example, Crawford & Platts[3] and Crawford[4] noted that downwind coned rotors for a 1.5 MW turbine can reduce loads in extreme wind conditions, especially if combined with hinges to allow the blades to be parked in a (horizontal) streamwise position. Examples of experimental studies of downwind rotors include Hand *et al.*[5] and Rasmussen *et al.*[6]

The most common concern about using a downwind rotor is the effect of the tower wake on the downstream blades, i.e. the "shadow effect." There is much uncertainty regarding the significance of the shadow effect on the rotor blades. Some researchers claim that the effect on the blades is negligible, while others claim that it has a large effect on the wind turbine performance. Zahle *et al.*[7] conducted a three-dimensional Navier-Stokes simulation to model the interaction between a wind turbine tower and a downwind rotor blade. They noted that when the blades were subjected to the velocity deficit in the tower wake they underwent a sudden deloading and subsequent reloading of forces. The sudden change in the aerodynamic loading on the blade may lead to a slight flutter every revolution. This effect may be compounded over the life span of the blade and result in significant blade fatigue, greatly increasing the chance for blade failure. As such, addressing the shadow effect is critical to achieving the potential benefits associated with a downwind rotor.

B. Previous Studies on Reducing Cylinder/Tower Wake

One possible solution for mitigating the impact that the tower wake has on the turbine blades is to employ active load control on the blades. Researchers at the University of California, Davis[8-9] have examined using a microtab-based load control system that is able to account for a 12% change in the freestream velocity. Unfortunately, the blade would have to have minimal lag response to be effective and is complicated by the fact that it must operate a rotating element at high-speed. Therefore, techniques to minimize the tower wake itself are preferred.

To reduce tower wake, one may employ an aerodynamically faired tower. Such a fairing can have a substantial impact because the drag (and thus strength of the turbulent wake) of an airfoil of a given thickness is many times less than that of a cylinder of the same thickness/diameter. This concept has been qualitatively tested by NREL.[10] A tower fairing can also be allowed to rotate freely about the fixed tower, as shown in Fig. 1 so that it will ideally always be aligned with the wind direction without requiring any significant change of the tower structure.

Many techniques have been implemented in an attempt to reduce the drag of a cylinder. Lee *et al.*[11] installed a small control rod upstream of the cylinder, Mashud *et al.*[12] attached circular rings around the cylinder, and Sosa *et al.*[13] used three-electrode plasma actuators. All three of these techniques resulted in a drag reduction of approximately 25%. Hwang and Yang[14] were able to achieve greater success in reducing the cylinder drag by nearly 40% by installing one splitter plate upstream of the cylinder and another in the cylinder wake. Finally, Triyogi *et al.*[15] were able to reduce the drag of a cylinder by nearly 50% by installing an I-type bluff body upstream of the cylinder. While these flow control methods did reduce the cylinder drag, they were applied in the laminar flow regime (with modest Reynolds numbers). Furthermore, these reductions are far less than the more than order of magnitude drag reduction possible by placing an aerodynamic fairing around the cylindrical tower.

There have been airfoils designed specifically for use as fairings to minimize drag. Some of the most effective of these airfoils are the Eppler strut series, particularly the Eppler 862 (E862) and Eppler 863 (E863) airfoils[16]. However, the Eppler strut airfoils were designed to operate at low Reynolds numbers and zero degrees angle of attack so they may not perform as well at the higher Reynolds numbers and finite angles of attack associated with an extreme-scale wind turbine. A turbine tower fairing should take these considerations into account, along with the ability to self-yaw, in order to obtain the optimal fairing geometry.

There have been few computational studies for fairings designed for wind turbine towers. One study at the Masdar Institute of Science and Technology[17] simulated the interaction between the tower and rotor for a downwind design by comparing a NACA 0012 airfoil cross-section with a circular cross-section. The researchers observed that the airfoil shaped tower produced a smaller wake compared with the cylindrical towers, and had the least overall impact on rotor instability. However, it should be noted that their aerodynamically shaped tower had a substantially smaller thickness than the cylindrical tower and thus would not provide the same structural support. The study also

only looked at the case where the airfoil is aligned with the incoming flow, which ignores the changes in wind direction that a wind turbine tower experiences.

Perhaps the most relevant work to date is the study conducted by Reiso and Muskulus[18] in which they conducted simulations to determine the effect that various tower fairing geometries and blade properties have on both tower and blade loads for downwind offshore wind turbines. The simulations were only run at zero angle of attack conditions, and the author concludes that a detailed study of the tower wake at non-zero angles of attack is needed.

There is a similar dearth of experiments that investigated the wake unsteadiness of a wind turbine using an aerodynamically faired tower, since conventional turbines use an upwind design where the tower has little influence on the flow that the rotor experiences. Hand *et al.*[5] did take wake measurements for a faired tower with a downwind turbine configuration but only for parked blade conditions. One study by Calkins[19] investigated the aero/hydrodynamic traits of symmetrical sections for use as fairings on cylindrical components by running experiments in a wind tunnel. The study set forth a list of criteria that an ideal fairing geometry would have: 1) streamlined symmetric section for low drag, 2) position of maximum thickness location as close to leading edge as possible with center of rotation forward of the hydrodynamic center for weathervane stability, and 3) high thickness to chord ratio to reduce the net size of the fairing, and 4) separation free boundary layer. As with the previous studies, the experiments only focused on taking steady data at a zero angle of attack. Based on similar objectives, several airfoils were computationally analyzed to determine the best geometry for a 15 MW wind turbine tower fairing for a downwind wind turbine configuration.[20-21] However, experiments are needed to investigate the performance, especially with respect to flow separation at angle of attack since such characteristics are difficult to predict with simulations.

In summary of previous work in this area, there have been multiple studies on reducing the drag of a cylinder with a fairing, but no experimental studies targeted to an aerodynamic fairing for a wind turbine tower. Further more previous studies on fairing designs have focused on idealized conditions of zero angle of attack with investigation on only time-averaged drag. In contrast this is the first study to investigate the detailed wake profile for a wind turbine tower fairing and the first to obtain and analyze unsteady velocity field data in the wake. Moreover, the present study is the first to examine the wake characteristics at various downstream locations and non-zero angles of attack for fairings that met all the Calkins criteria, as specified above, and the first to provide comparisons to a simple cylinder.

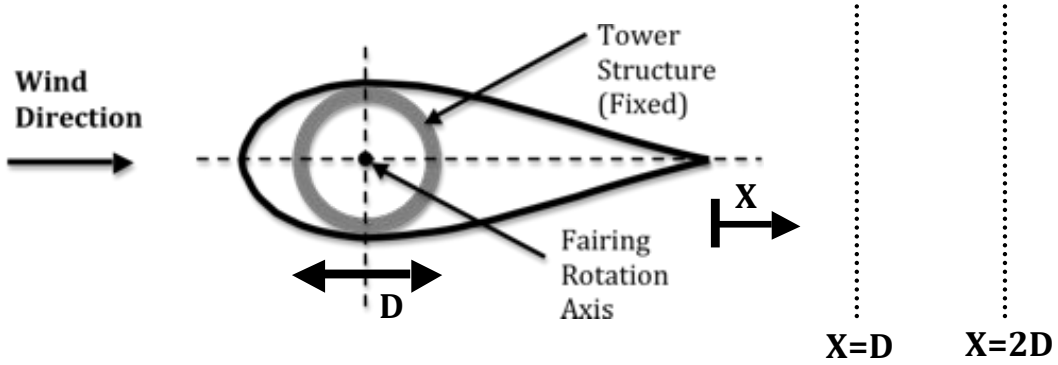

Figure 1. Schematic of cross-section of tower with fixed structure and rotatable aerodynamic fairing.

C. Objectives

The primary objective of these experiments is to evaluate select aerodynamic fairing geometries that can reduce the effects that the tower wake has on a downwind rotor. The ideal fairing would have: 1) minimum drag for a given thickness and wind speed (associated with wind turbine conditions) so as to reduce wake effects, 2) a small chord but should have an inscribed diameter consistent with the outer diameter of the tower, i.e. the fairing airfoil should have a small chord-to-diameter ratio, 3) a self-correcting moment about the tower center when at finite angles of attack to allow self-alignment, and 4) significant robustness as measured by its ability to prevent flow separation at significant angles of attack. The selected fairing designs already meet the second and third objectives, therefore theses experiments are focused on analyzing the ability of the fairing to prevent flow separation and minimize the velocity deficit in the tower wake. Flow separation of the fairing can lead to a large increase in both the drag and wake turbulence of the tower that would negatively impact the turbine rotor. Reducing the velocity deficit reduces the dynamic unloading and loading of rotor blades as they pass through the tower wake, thereby reducing the

potential for undesirable flutter. These experiments are the first to test fairing geometries with respect to these criteria specifically for use with wind turbine towers.

II. Experimental Methods

A. Flow Visualization

Flow visualization is a simple experimental technique where a visible substance is introduced into the flow so that the flow dynamics can be observed. Flow visualization is generally more useful for acquiring qualitative results than quantitative results. The tracer substance must be able to follow the flow, and for this reason dyes are most commonly used in water and smoke is most commonly used in air.[22] Solid or gaseous tracers as well as floating agents may also be used for flow visualization in water, but liquid tracers, such as dyes, are best suited to follow the flow.[23] Using flow visualization to observe aerodynamic flow phenomena in a water tunnel has the advantage that at the same Reynolds number the flow can be observed at a slower speed.[24]

B. Particle Image Velocimetry

PIV is a non-intrusive method for measuring instantaneous velocities in a flow field. Unlike other techniques that require probes in the flow to take measurements, PIV does not disrupt the flow field it is measuring. For PIV, the flow is seeded with small tracer particles that follow the flow exactly. A laser beam passes through a series of lenses to produce a laser sheet, and the laser sheet is used to illuminate the particles in the area of interest. The laser is synchronized with a camera, and two pulses from two aligned lasers are fired in quick succession to capture two images of the particles with a known time between them. The PIV software uses the two images to determine the distance each illuminated particle traveled in the given time and calculates the particle velocity. Each image is broken up into individual interrogation spots, and all of the particle velocities in an interrogation spot are averaged into a single velocity vector. The velocity vectors from all of the interrogation windows are combined to create an instantaneous velocity field. A large number of these instantaneous fields can be averaged to determine the average flow field.

C. Experimental Setup

In the computational analysis, the Eppler strut airfoils, particularly the E863, exhibited the best performance. The C30u design had the best performance of the remaining airfoils that were considered. Models of the E863 and the C30u airfoils were created for the experiments. A schematic of the airfoil geometries are shown in Fig. 2. The airfoil models were made of ABS plastic using a 3-D printer. The Reynolds number for the experiments is significantly lower than the full-scale Reynolds number, so the airfoil models had to be made as large as possible, to maximize the Reynolds number, without introducing significant blockage effects. This resulted in a maximum airfoil thickness of 67 mm. The models were sanded and painted with a polyurethane coating to give them a smooth surface. A cylinder with a diameter equal to the thickness of the airfoil models was also used as a baseline to compare the performance of the airfoils.

The experiments were conducted in a water channel located at the University of Virginia. The water channel has a maximum flow velocity of 1 m/s. Ideally the maximum flow velocity would be used to maximize the Reynolds number, but the higher flow velocities introduced unwanted free surface effects, as seen in Fig. 3a. These effects are even greater at larger angles of attack, and for a nose-up orientation, the curvature of the free surface can help keep the boundary layer attached when it would normally separate. To help reduce the effects of the free surface on the flow, the angles of attack herein are defined as positive for a nose-down orientation. Since all of the airfoils in the experiments are symmetric, the performance is the same at positive and negative angles of attack. It was determined that a flow velocity of 0.5 m/s was the maximum velocity that did not introduce significant free surface effects, as seen in Fig. 3b. A steady state inflow was used, because, as this is the first study of its kind, the idealized conditions must be analyzed before adding the increased complexity that comes with a turbulent inflow.

The Reynolds number based on the inscribed diameter for the models turned out to be $Re_D = 3.35 \times 10^4$, which is two orders of magnitude lower than the full-scale Reynolds number of $Re_D = 8.33 \times 10^6$. To help compensate for the disparity in the Reynolds number, a trip strip was placed near the leading edge of the models to trip the laminar boundary layer to the turbulent regime. While the difference in the Reynolds number means that the experiments will not fully predict the flow of the full-scale system, the experiments are still useful for comparing the two airfoils to determine which is the best design.

The experiments were conducted at angles of attack of 0° and 10°. Since the tower fairing will self align with the wind direction, the maximum angle that the fairing will experience will be less than the maximum change in the

wind direction. The self-aligning property of the fairing makes it probable that the fairing will not experience angles greater than 10° for significant periods of time.

The influence of the water channel walls must be taken under consideration. The calculations for the tunnel corrections were taken from Selig and McGranahan.[25] The corrected angle of attack is calculated, *viz*

$$\alpha_c = \alpha + \frac{57.3\sigma}{2\pi}\left(C_{l,u} + 4C_{m,c/4,u}\right) \tag{1}$$

where α_c is the corrected angle of attack, α is the physical angle of attack, $C_{l,u}$ is the uncorrected lift coefficient, $C_{m,c/4,u}$ is the uncorrected moment coefficient about the quarter chord, and σ is the tunnel correction parameter calculated by

$$\sigma = \frac{\pi^2}{48}\left(\frac{c}{h}\right)^2 \tag{2}$$

where c is the airfoil chord length and h is the height of the test section. For the 0° angle there is no correction that needs to be made because the lift and moment coefficients are both zero. For the 10° cases, the corrected angle was calculated to be 10.30° for the C30u, and 10.08° for the E863. These angle corrections are minimal and should not have a significant effect on the results.

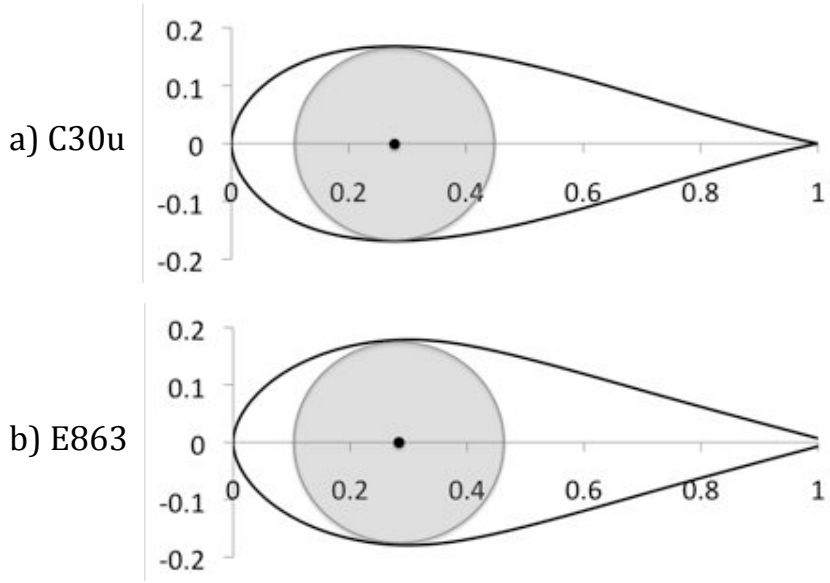

Figure 2. Schematics of the selected airfoils with the tower located at the maximum thickness.

a) 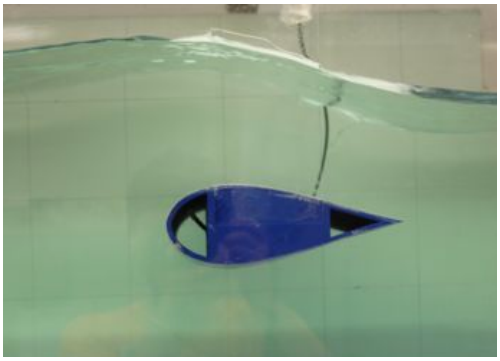 b) 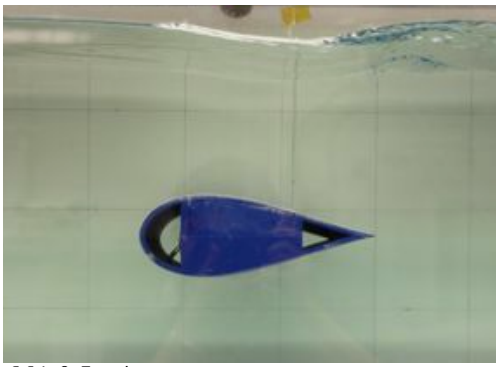

Figure 3. Water channel free surface effect at a) 0.8 m/s, and b) 0.5 m/s.

D. Flow Visualization Setup

The flow visualization experiments were conducted using direct injection of a water-based dye. The dye system uses pressure regulation to control the dye flow rate. The dye was injected into the flow through a tube that passed through the inside of the airfoil to a hole in the bottom surface of the airfoil near the leading edge. Passing the tube through the airfoil instead of placing the tube directly in the flow ensures that the flow is not disturbed. The dye was injected at a low velocity to ensure that the dye accurately follows the flow. The flow visualization experiments were used primarily to investigate flow separation at various angles of attack.

E. Particle Image Velocimetry Setup

PIV measurements were taken for five cases: a cylinder, the C30u at 0° and 10°, and the E863 at 0° and 10°. A schematic of the PIV setup is shown in Fig. 4. The flow was seeded using hollow glass spheres with diameters of 8-12 μm. For the C30u and E863 cases, the laser sheet was positioned behind the airfoil to capture the wake region, and the camera was positioned so that the trailing edge of the airfoil was barely out of view to the left of the interrogation window. For the cylinder case, the laser sheet and interrogation window were positioned such that the distance from the cylinder to the interrogation window is the same as the distance from the maximum thickness of the airfoils to the interrogation window.

The PIV experiments were conducted using a New Wave Nd: Yag Solo PIV III laser with a pulse duration of 3-5 ns, pulse frequency of 7 Hz and pulse energy of 150 mJ. The camera was a TSI PowerView Plus with a 2048x2048 resolution. The time step for each case was chosen to maximize the percentage of good vectors collected, which typically occurs when the particles travel approximately 1/4 of the interrogation spot size. The time step varied between 200 and 600 μs depending on the test case. The images were processed with the Insight 4G software from TSI. The processing was done using Insight 4G for a two image cross correlation with a Nyquist grid with an interrogation spot size of 64x64 pixels. Post-processing was used to eliminate any vectors that were outside of the velocity tolerance of the local median velocity. The PIV setup was able to produce approximately 80% good vectors. The majority of the error occurred around the edges where particles can leave and enter the interrogation window between the two images. Five hundred image pairs were captured for each case to calculate the average flow field. Uzol and Camci[26] conducted a study on the effect of sample size on the averaged PIV measurements. For the flow field that was studied, increasing the sample size beyond 500 image pairs had little effect on the accuracy of the average flow field. The PIV results were used to display the instantaneous velocity, average velocity, and average turbulence fields of the model wakes. MATLAB was used to plot the u- and v-velocity profiles at fixed X locations of one and two diameters downstream of the left edge of the interrogation window.

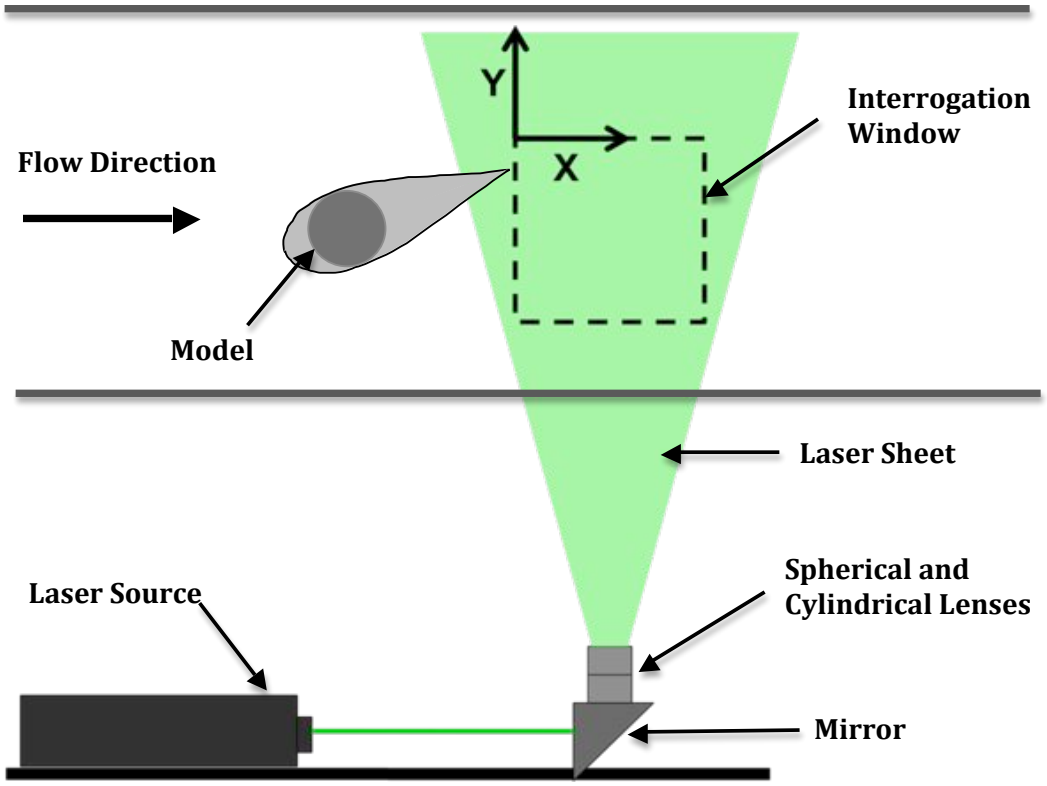

Figure 4. Schematic of PIV Setup.

III. Experimental Results

A. Flow Visualization Results

The flow visualization experiments provide a qualitative analysis of flow separation. The Reynolds number in the water channel is lower than the full-scale Reynolds number, so the full-scale fairing is expected to have less separation than the results shown here. The flow visualization experiments are still useful for comparing the fairing designs.

Figure 5 shows the dye images for the C30u airfoil at 0° and 10°. At 0° there appears to be a small separation bubble, but otherwise the flow remains attached, while at 10° the flow is separated. Figure 6 shows the dye images for the E863 airfoil at 0° and 10°. At 0° the boundary layer remains attached, while the flow is separated at 10°.

At 0° the C30u has a small separation bubble that the E863 does not have, but the E863 has a thicker boundary layer that would result in a thicker wake. Both airfoils appear to have a similar performance at 10°. Both airfoils were also observed at 5°, but there was no apparent distinction between the two airfoils. Overall the airfoils appear to perform equally with respect to flow separation, although tests should be run closer to the full-scale Reynolds number to verify this.

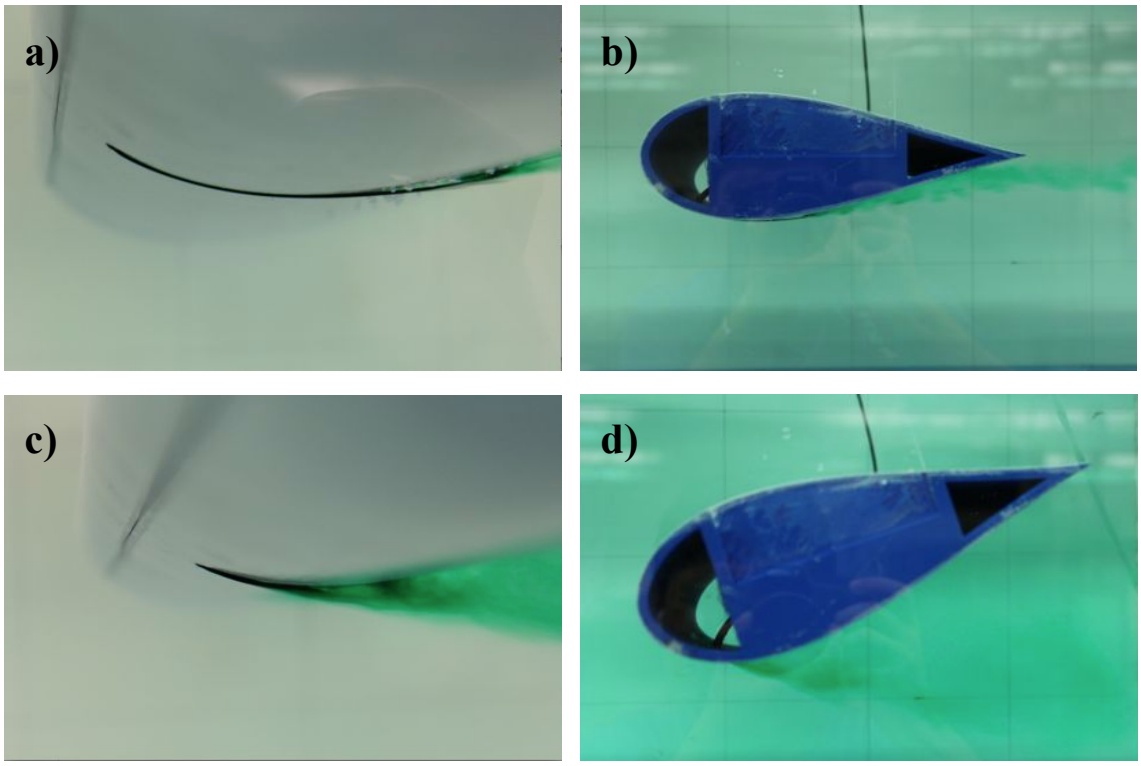

Figure 5. Dye images for the C30u at: a-b) 0° angle of attack and c-d) 10° angle of attack.

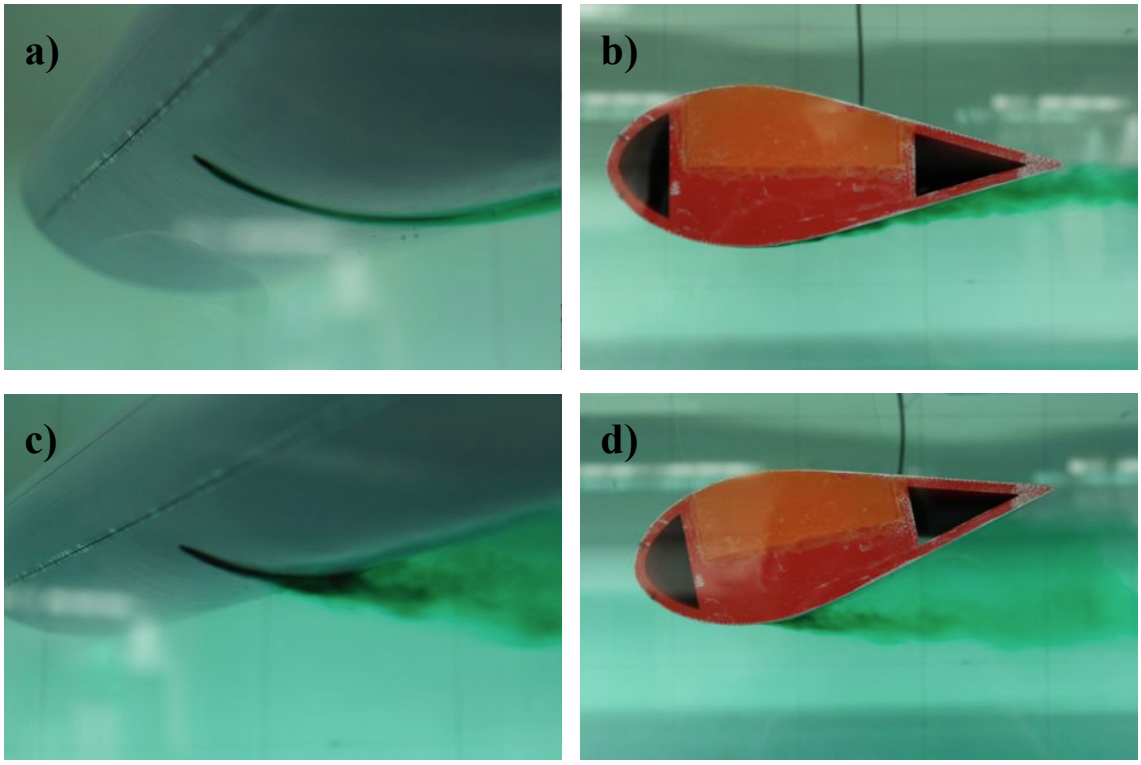

Figure 6. Dye images for the E863 at: a-b) 0° angle of attack and c-d) 10° angle of attack.

B. Particle Image Velocimetry Results

The PIV experiments were used to analyze the wake of the two airfoils compared to the wake of a cylinder. Figures 7 shows an example instantaneous velocity vector map for the cylinder produced by the PIV experiments. Figure 8 shows the instantaneous velocity contours in the wake of each model at 0° and 10°. At 0°, both airfoils have a thin wake with a small velocity deficit, while the cylinder displays a thick wake region with large turbulent eddies. At 10°, both airfoil wakes exhibit turbulent behavior, and the wake region is much larger than the 0° case, although they are still smaller than the cylinder wake region.

The averaged wake velocity contours at 0° and 10° are shown in Fig. 9 while the turbulence contours at 0° and 10° are shown in Fig. 10. At 0°, both airfoils have a significantly thinner wake and lower turbulence than the cylinder. The cylinder has a region of high turbulence at the location farthest upstream of the interrogation window that slowly dies out farther downstream. The C30u appears to have a thinner wake and lower turbulence than the E863, but the differences are minimal. At 10°, the velocity fields of the two airfoils are similar, with both airfoils exhibiting a recirculation zone. The wake thickness of both airfoils has increased, but they are still thinner than the cylinder wake. At the farthest upstream point, the airfoils have significantly lower turbulence than the cylinder, but the differences are less noticeable farther downstream. The airfoils have similar turbulence levels, but the C30u has less turbulence at the top and bottom of the interrogation window.

The u-velocity profiles at angles of attack of 0° and 10° for two fixed X locations are shown in Figs. 11 and 12. Figure 11 shows the velocity profiles at a distance one diameter downstream, and Fig. 12 shows the velocity profiles two diameters downstream. It is important to consider the scatter of the data points as well as the average because the rotor blades must be able to handle the extreme cases that cannot be seen by just examining the average distribution. At 0°, both airfoils have a very thin wake with a small velocity deficit. The cylinder wake extends nearly the entire height of the interrogation window and has a larger velocity deficit than the airfoils. There is only a slight deviation from the mean velocity for the airfoils at this angle of attack, while the deviation is significant for the cylinder. The C30u appears to have a slightly smaller velocity deficit than the E863. The velocity deficits of the airfoils' wakes are reduced farther downstream, but the velocity deficit of the cylinder appears to remain unchanged downstream. At 10°, both airfoils have a significantly thicker wake and larger velocity deficit than at 0°. The wake thicknesses and velocity deficits appear to be approximately equal for both airfoils. At the farther upstream location, the airfoils have larger average velocity deficits than the cylinder, but they also have thinner wakes. At the farther downstream location, the average velocity deficit of the airfoils is approximately the same as the velocity deficit of the cylinder, but the airfoils have thinner wakes. At both locations, the scatter for the airfoils and the cylinder is approximately the same in the middle of the wake, but the airfoils have significantly less scatter near the edges of the wake. This means that the time that the passing rotor blade may be affected by the wake is reduced when using a tower fairing. An important observation to note is that when the airfoils are at 10° at the farther upstream location, even though the average u-velocity is positive, a significant number of data points show a negative velocity that could have an adverse effect on the rotor blades.

The v-velocity profiles at angles of attack of 0° and 10° are shown in Figs. 13 and 14. Figure 13 shows the velocity profiles at a distance one diameter downstream, and Fig. 14 shows the velocity profiles two diameters downstream. At 0°, all of the models had an average v-velocity of zero, but the cylinder experiences significant variations in the velocity that are not present for the C30u and E863. The C30u has a lower deviation from the mean in the airfoil wake than the E863. At 10°, the variation in the v-velocity of the airfoils is only slightly less than the variation in the velocity of the cylinder wake, but the variations occur over a thinner region. At the farther upstream location, the average v-velocity for both airfoils is negative in the upper half of the interrogation window and positive in the lower half. This effect is reduced farther downstream and is almost negligible two diameters downstream. There are no significant differences between the wake velocities of the two airfoils at this angle of attack.

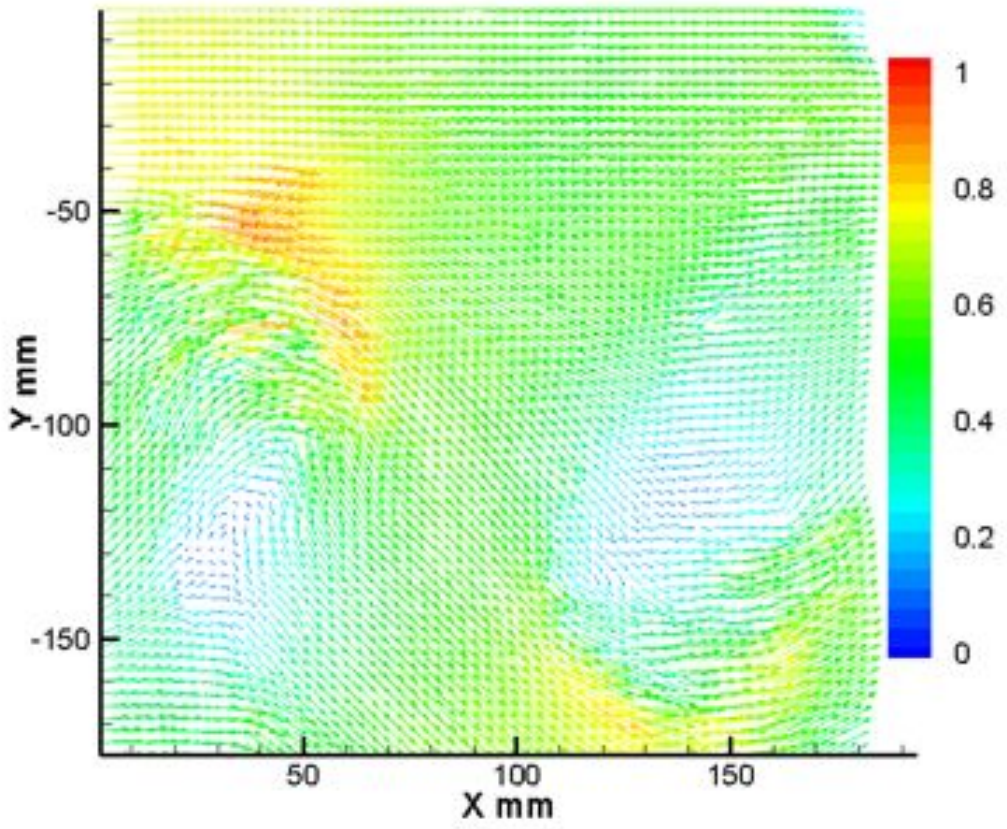

Figure 7. Example instantaneous velocity (in m/s) vector map for the cylinder.

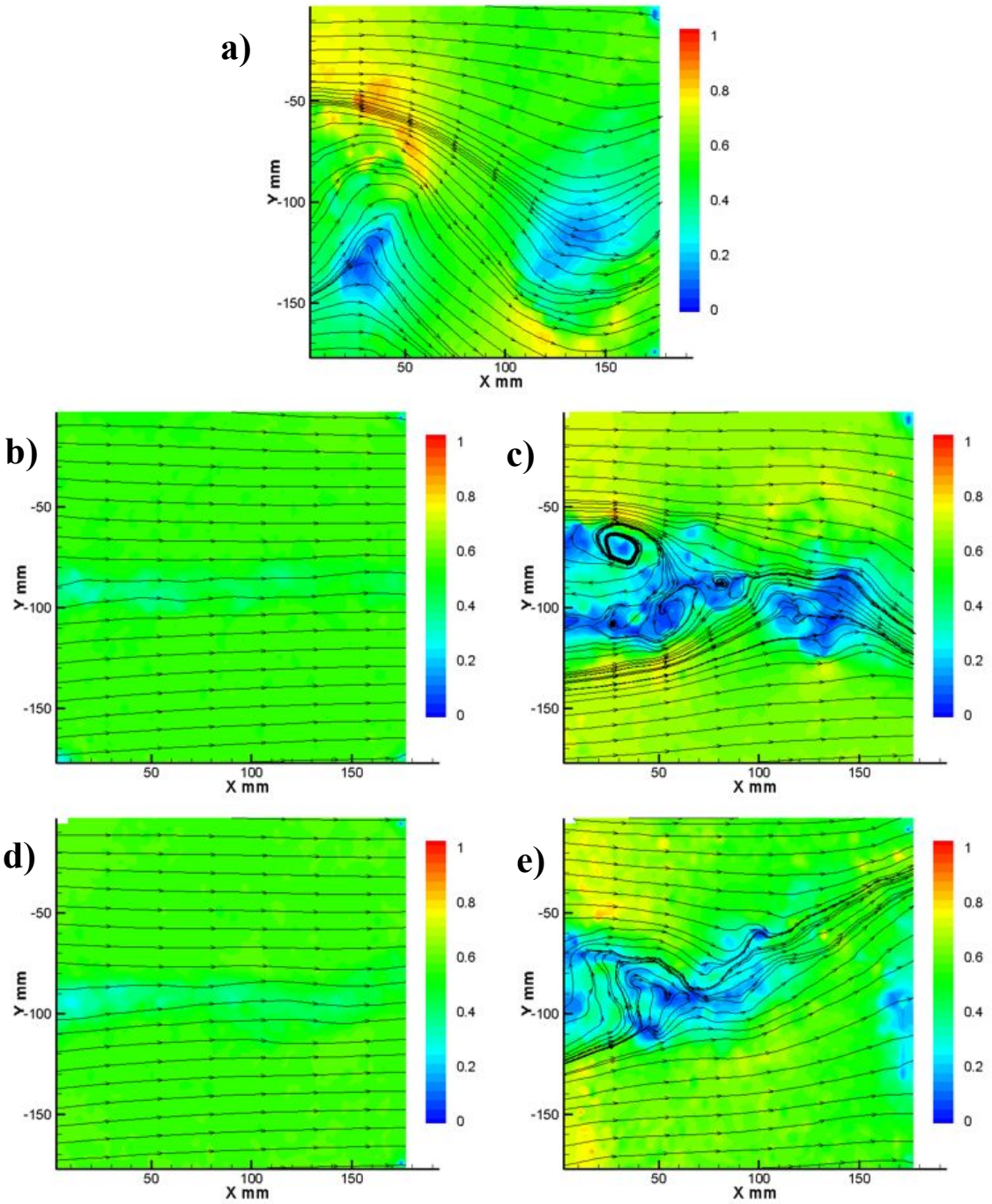

Figure 8. Instantaneous velocity contours (in m/s) for: a) the cylinder, b) the C30u airfoil at 0°, c) the C30u airfoil at 10°, d) the E863 airfoil at 0°, and e) the E863 airfoil at 10°.

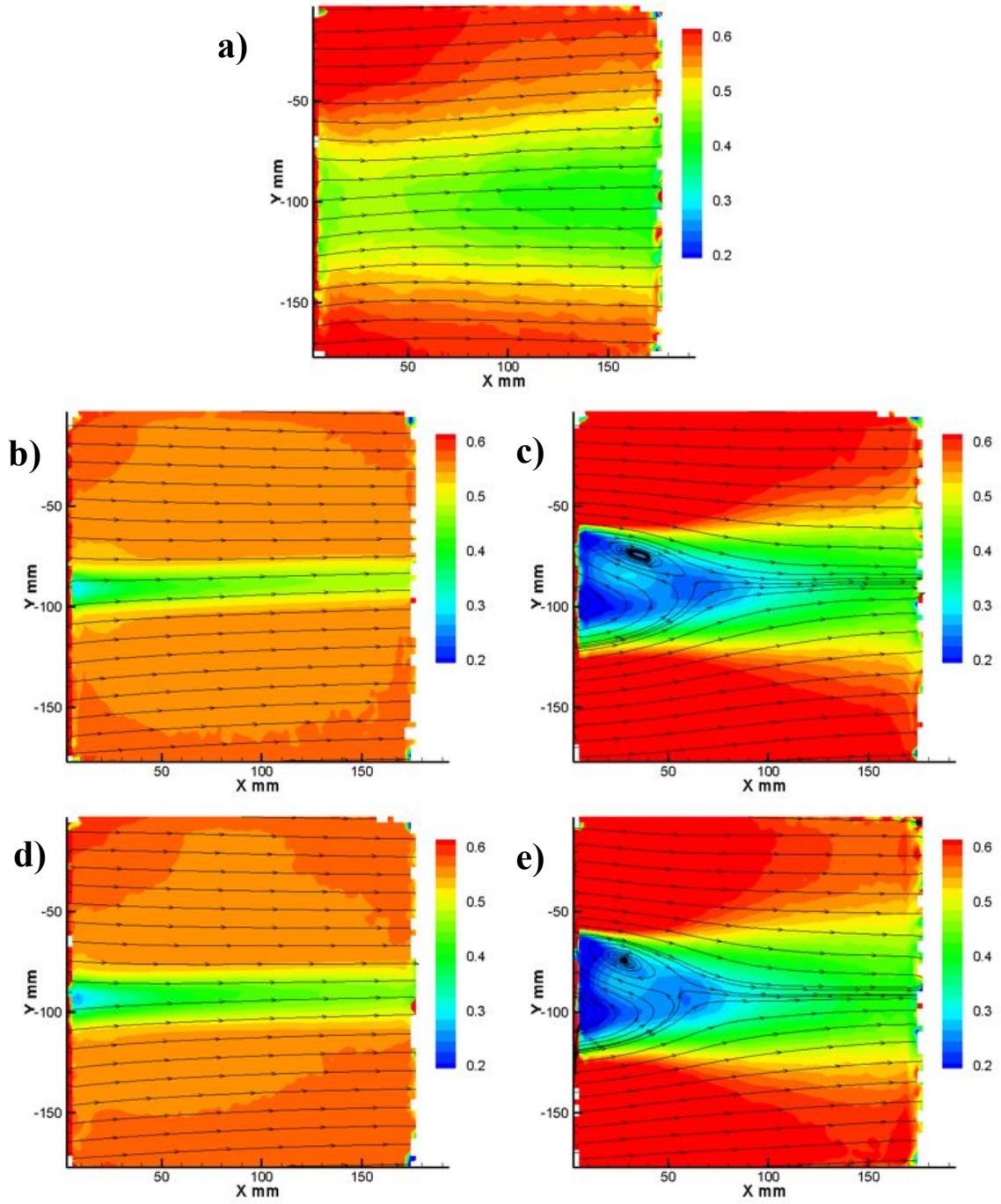

Figure 9. Average velocity contours (in m/s) for: a) the cylinder, b) the C30u airfoil at 0°, c) the C30u airfoil at 10°, d) the E863 airfoil at 0°, and e) the E863 airfoil at 10°.

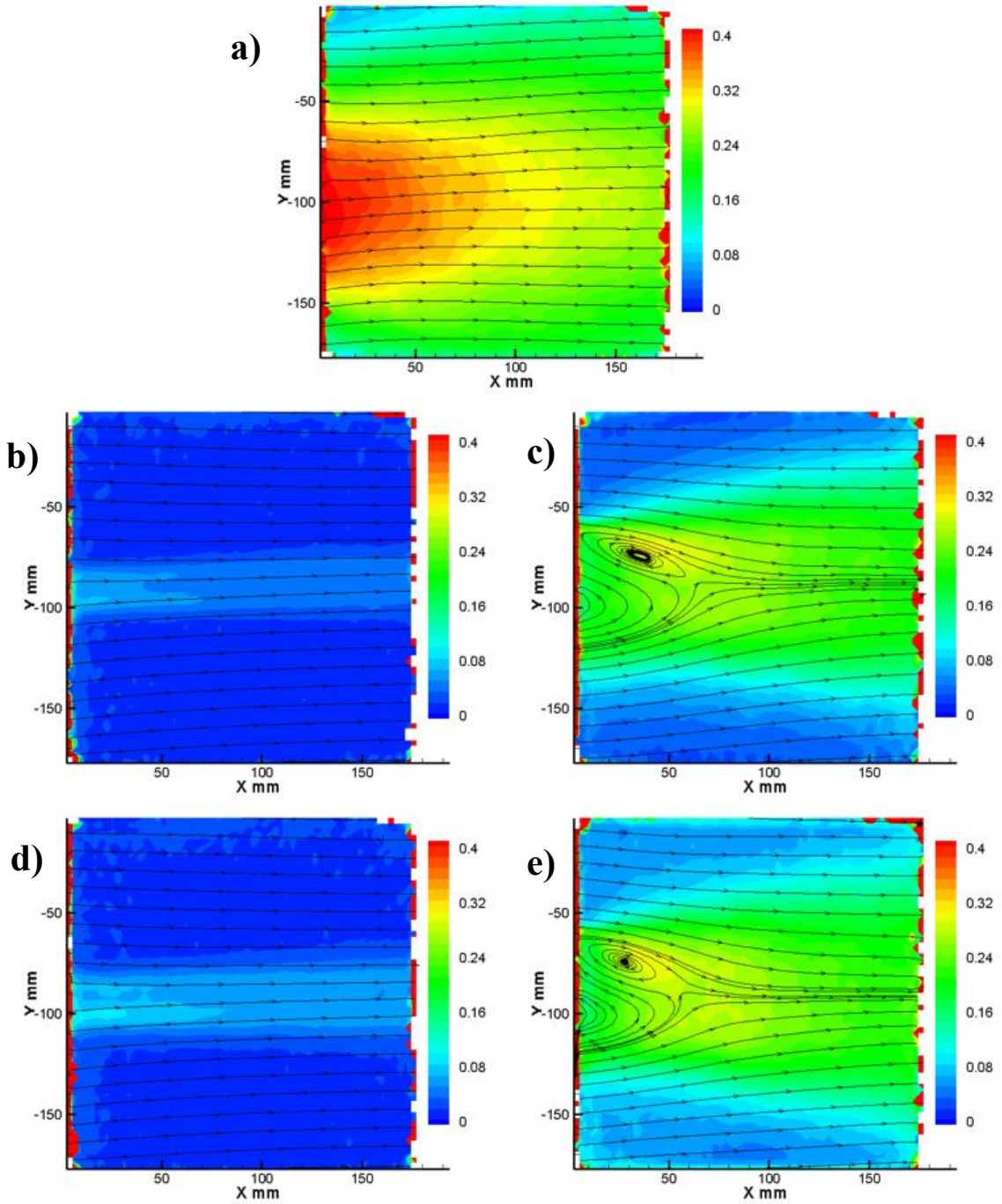

Figure 10. Average turbulence contours (in m/s) for: a) the cylinder, b) the C30u airfoil at 0°, c) the C30u airfoil at 10°, d) the E863 airfoil at 0°, and e) the E863 airfoil at 10°.

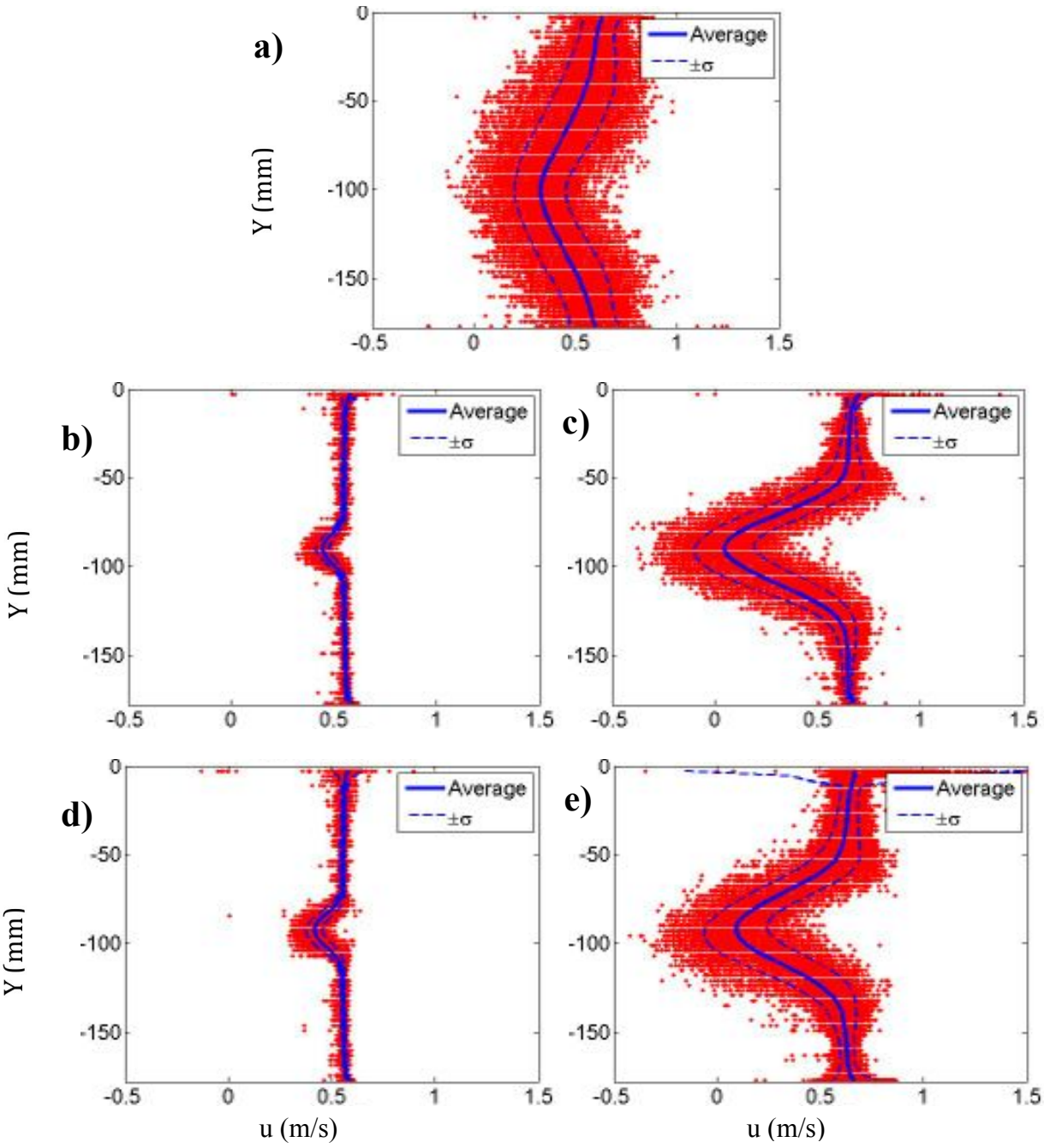

Figure 11. *u*-velocity profile one diameter downstream for: a) the cylinder, b) the C30u airfoil at 0°, c) the C30u airfoil at 10°, d) the E863 airfoil at 0°, and e) the E863 airfoil at 10°.

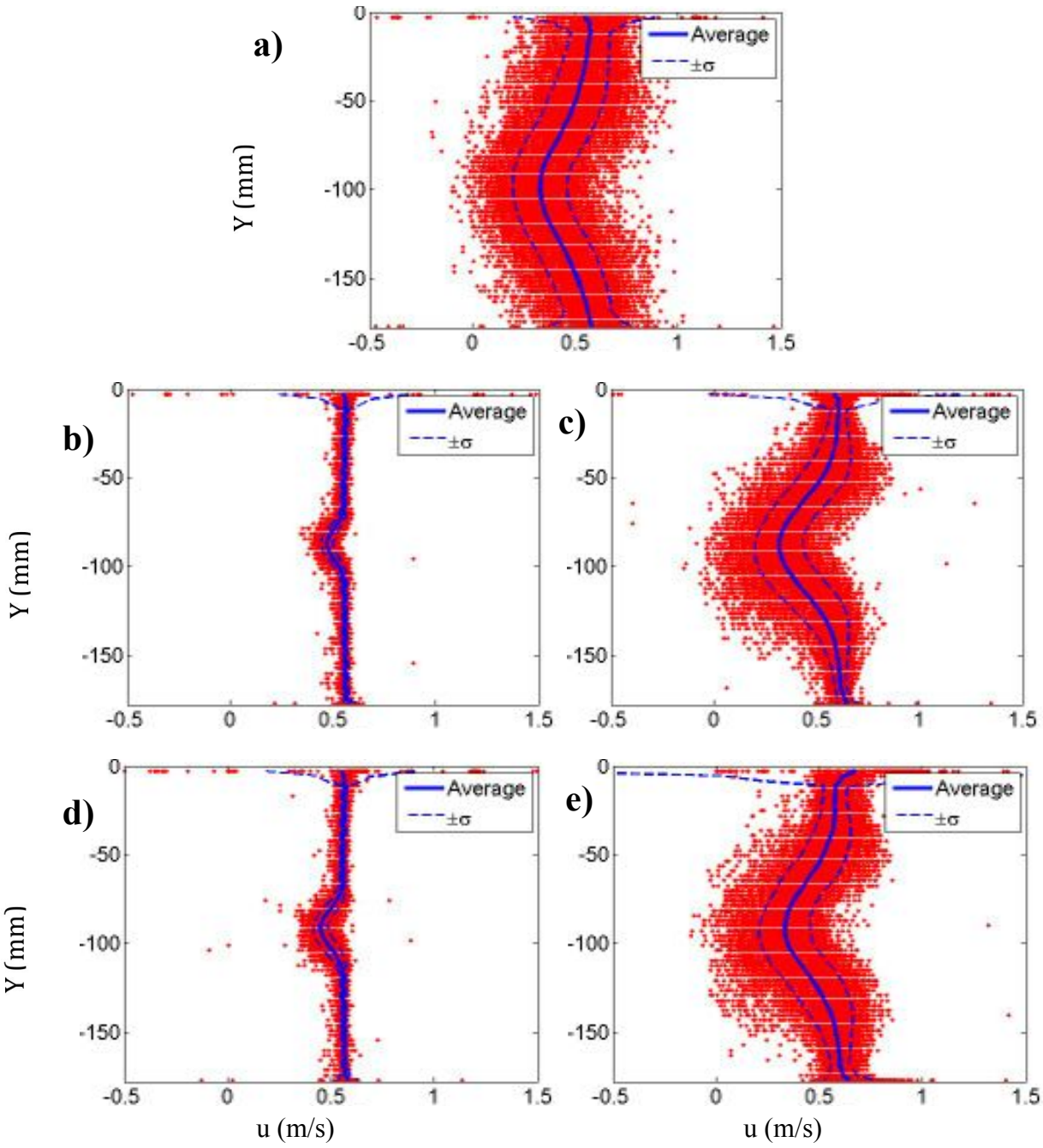

Figure 12. *u*-velocity profile two diameters downstream for: a) the cylinder, b) the C30u airfoil at 0°, c) the C30u airfoil at 10°, d) the E863 airfoil at 0°, and e) the E863 airfoil at 10°.

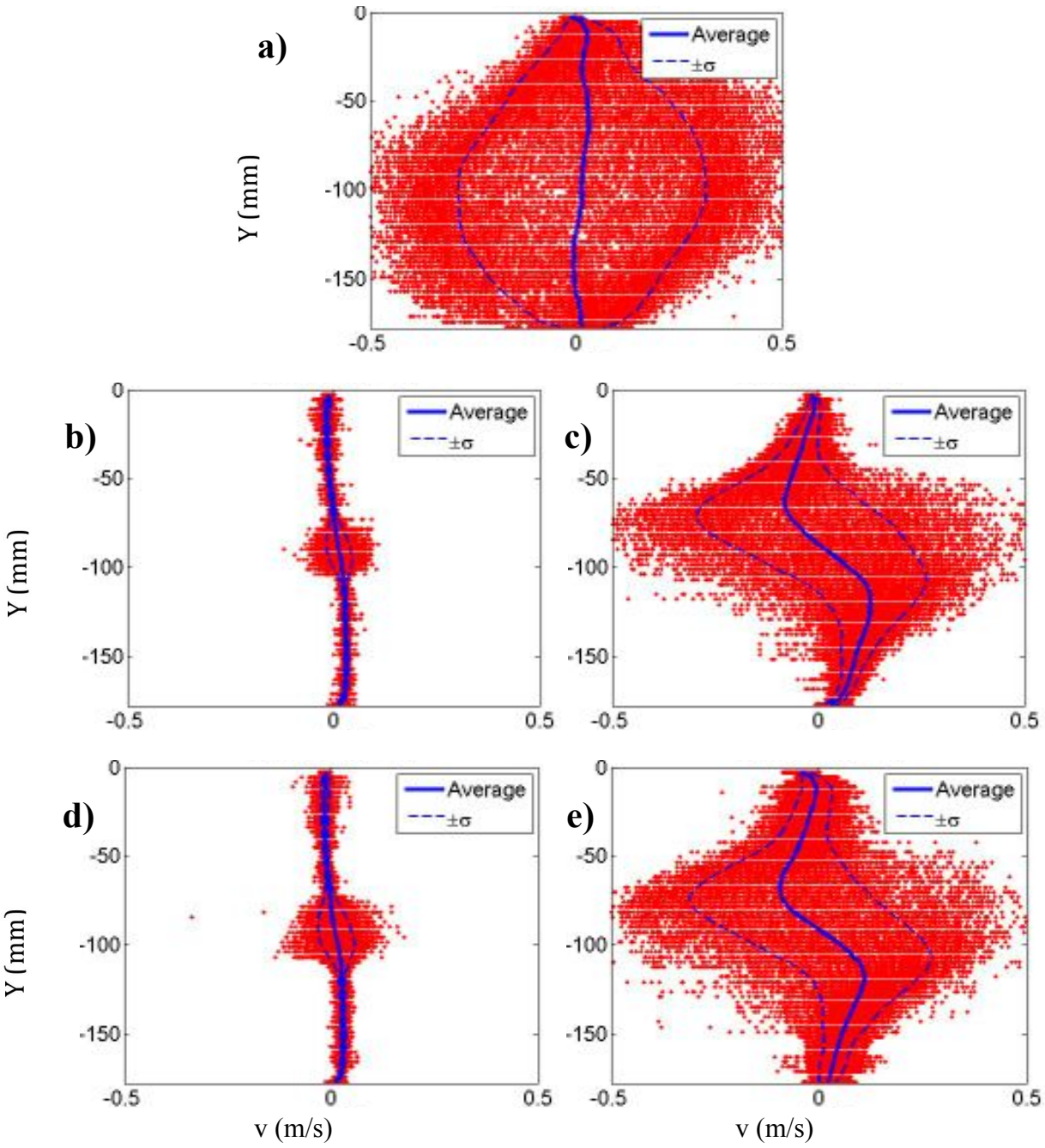

Figure 13. *v*-velocity profile one diameter downstream for: a) the cylinder, b) the C30u airfoil at 0°, c) the C30u airfoil at 10°, d) the E863 airfoil at 0°, and e) the E863 airfoil at 10°.

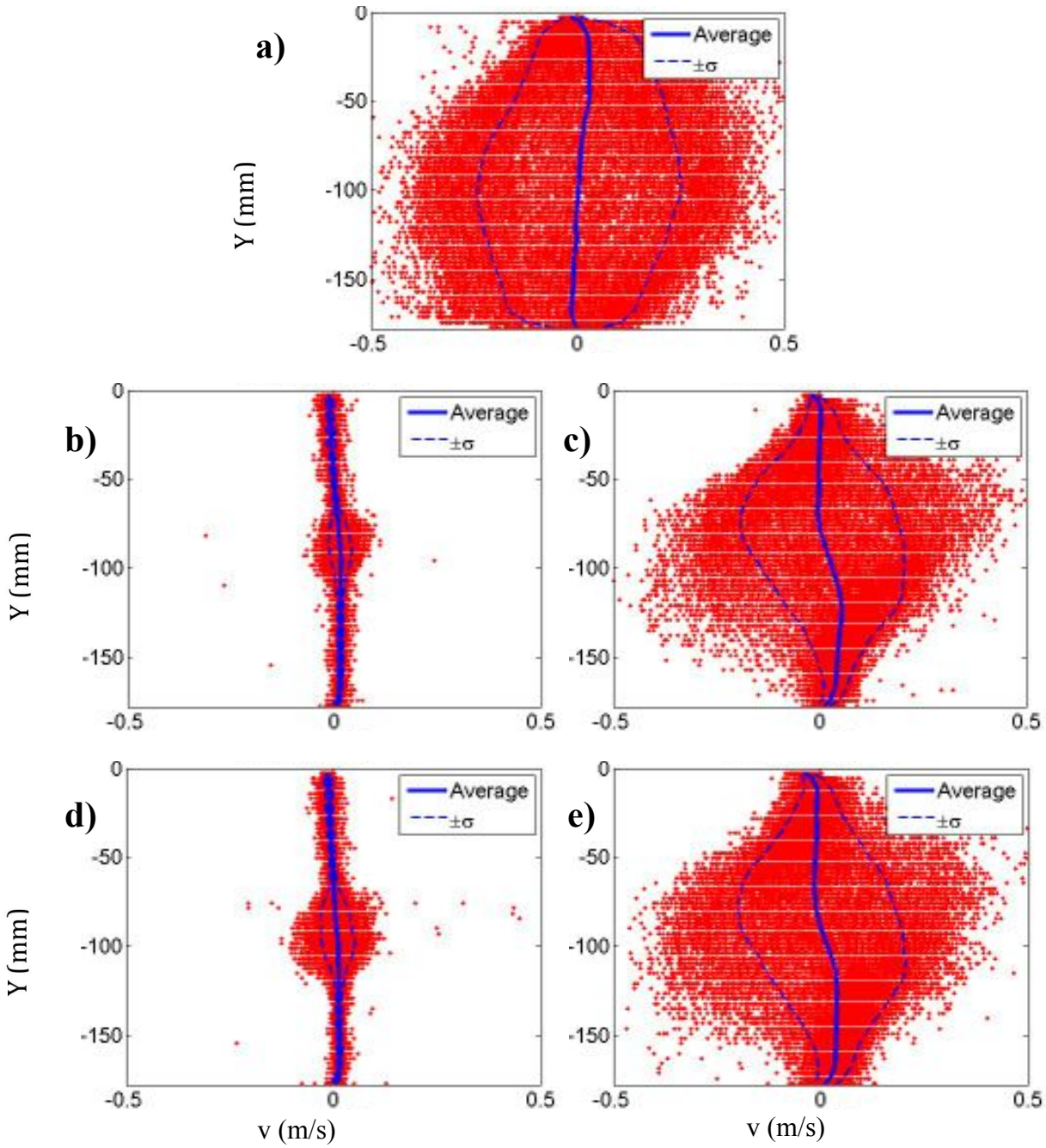

Figure 14. *v*-velocity profile two diameters downstream for: a) the cylinder, b) the C30u airfoil at 0°, c) the C30u airfoil at 10°, d) the E863 airfoil at 0°, and e) the E863 airfoil at 10°.

IV. Conclusions

Flow visualization and PIV were used to analyze flow separation and wake effects of two airfoils at 0° and 10°. The flow visualization results showed that both the C30u and E863 airfoils had similar performances with respect to flow separation. At 0°, the flow remained attached, but at 10° the flow separated for both airfoils. The Reynolds number for the experiments is two orders of magnitude less than the full-scale Reynolds number, so the flow is more likely to remain attached for the full-scale fairing. At 0°, the C30u appeared to have a small separation bubble that the E863 did not have, but the E863 had a thicker boundary layer than the C30u. Other than those differences at 0°,

the dye experiments showed no discernable differences between the two airfoils. Further tests with a Reynolds number closer to the full-scale would be useful to distinguish the two airfoils.

From the PIV results it appeared that there were few differences between the performances of the C30u and E863 airfoils. At 0°, the C30u appeared to perform slightly better than the E863, while at 10°, both airfoils appeared to have approximately equal performance. The wake effects of the C30u and E863 airfoils were significantly lower than the cylinder wake effects at 0°. At 10°, the airfoils performed slightly better than the cylinder, but the advantages of the tower fairing are not as pronounced at this angle of attack as they are at 0°. Due to the self-aligning nature of the fairing it should not experience large angles of attack for long periods of time, therefore a tower fairing could be used to significantly reduce the effects of the tower wake on the wind turbine blades. If a tower fairing is used, it is suggested that the rotor plane is placed at least two tower diameters downstream of the fairing trailing edge, both for the reduced wake effects at this distance as well as to avoid any negative *u*-velocity components that may adversely affect the turbine performance.

One of the main factors for the reduced performance of the airfoils compared to the cylinder at higher angles of attack is most likely due to the flow separation that was observed in the dye experiments. At the full-scale Reynolds number, the flow around the airfoils is more likely to remain attached, while the flow around the cylinder may still separate. Experimental testing at higher Reynolds numbers is suggested to better predict the performance of the tower fairing designs.

References

[1]Ichter, B., Steele, A., Loth, E., and Moriarty, P., "Structural Design and Analysis of a Segmented Ultralight Morphing Rotor (SUMR) for Extreme-Scale Wind Turbines," *AIAA Fluid Dynamics Conference*, AIAA Paper 2012-3270, New Orleans, LA, June 2012.

[2]Loth, E., Steele, A., Ichter, B., Selig, M.S., and Moriarty, P., "Segmented Ultralight Pre-Aligned Rotor for Extreme-Scale Wind Turbines," *AIAA Aerospace Sciences Meeting*, AIAA Paper 2012-1290, Nashville, TN, Jan. 2012.

[3]Crawford, C., Platts, J., "Updating and Optimization of a Coning Rotor Concept," *Journal of Solar Energy Engineering*, Vol. 130, No. 3, 2008.

[4]Crawford, C., "The Path from Functional to Detailed Design of a Coning Rotor Wind Turbine Concept," *Proceedings of the Canadian Engineering Education Association*, 2011.

[5]Hand, M., Simms, D., Fingersh, L.J., Jager, D.W., Cotrell, J.R., Schreck, S., and Larwood, S.M., "Unsteady Aerodynamics Experiment Phase VI: Wind Tunnel Test Configurations and Available Data Campaigns," NREL/TP-500-29955, Golden, CO, Dec. 2001.

[6]Rasmussen, F., Petersen, J.T., Volund, P. Leconte, P, Szechenyi, E., and Westergaard, C., "Soft Rotor Design for Flexible Turbines," Risø National Laboratory, Roskilde, Denmark, Contract JOU3-CT95-0062.

[7]Zahle, F., Sørensen, N.N., and Johansen, J., "Wind Turbine Rotor-Tower Interaction Using an Incompressible Overset Grid Method," *Wind Energy*, Vol. 12, No. 6, Sep. 2009, pp. 594-619.

[8]Baker, J.P., Standish, K.J., and van Dam, C.P., "Two-Dimensional Wind Tunnel and Computational Investigation of a Microtab Modified Airfoil," *Journal of Aircraft*, Vol. 44, No.2, 2007, pp. 563-572.

[9]Cooperman, A.M., Chow, R., and van Dam, C.P., "Active Load Control of a Wind Turbine Airfoil Using Microtabs," *Journal of Aircraft*, Vol. 50, No. 4, 2013, pp. 1150-1158.

[10]Moriarty, P., Personal Communication, January 24, 2014.

[11]Lee, S.J., Lee, S.I., and Park, C.W., "Reducing the Drag on a Circular Cylinder by Upstream Installation of a Small Control Rod," *Fluid Dynamics Research*, Vol. 34, No. 4, Apr. 2004, pp. 233-250.

[12]Mashud, M., Islam, M.S., Bari, G.S., and Islam, M.R., "Reduction of Drag Force for a Cylinder by Attaching Cylindrical Rings," *Asian Congress of Fluid Mechanics*, Dhaka, Bangladesh, Dec. 2010, pp. 174-177.

[13]Sosa, R., D'Adamo, J., and Artana, G., "Circular Cylinder Drag Reduction by Three-Electrode Plasma Actuators," *Journal of Physics: Conference Series*, Vol. 166, No. 1, 2009.

[14]Hwang, J.Y. and Yang, K.S., "Drag Reduction on a Circular Cylinder Using Dual Detached Splitter Plates," *Journal of Wind Engineering and Industrial Aerodynamics*, Vol. 95, No. 7, July 2007, pp. 551-564.

[15]Triyogi, Y., Suprayogi, D., and Spirda, E., "Reducing the Drag on a Circular Cylinder by Upstream Installation of an I-type Bluff Body as Passive Control," *Journal of Mechanical Engineering Science*, Vol. 223, Oct. 2009, pp. 2291-2296.

[16]Eppler, R., *Airfoil Design and Data*, Springer-Verlag Berlin Heidelberg, 1990.

[17]Janajreh, I., Talab, I., and Macpherson, J., "Numerical Simulation of Tower Rotor Interaction for Downwind Wind Turbine," *Modelling and Simulation in Engineering*, 2010.

[18]Reiso, M., Muskulus, M., "The simultaneous effect of a fairing tower and increased blade flexibility on a downwind mounted rotor," *Journal of Renewable and Sustainable Energy*, Vol. 5, 033106, May 2013.

[19]Calkins, D.E., "Two-Dimensional Hydrodynamic Characteristics of a Bluff Symmetrical Fairing Section," *AIAA Journal*, Vol. 22, No. 9, Sep. 1984, pp. 1216-1221.

[20]O'Connor, K., Loth, E., and Selig, M.S., "Design of a 2-D Fairing for a Wind Turbine Tower," *AIAA Applied Aerodynamics Conference*, San Diego, CA, June 2013.

[21]O'Connor, K., *Development and Testing of a Fairing for a Wind Turbine Tower,* M.S. Thesis, University of Virginia, 2014.

[22]Merzkirch, W., "Techniques of Flow Visualization," AGARD Report, Dec. 1987.

[23]Werlé, H., "Hydrodynamic Flow Visualization," *Annual Review of Fluid Mechanics,* Vol. 5, Jan. 1973, pp. 361-382.

[24]Erickson, G.E., "Water Tunnel Flow Visualization: Insight into Complex Three-Dimensional Flowfields," *Journal of Aircraft,* Vol. 17, No. 9, 1980, pp. 656-662.

[25]Selig, M.S. and McGranahan, B.D., "Wind Tunnel Aerodynamic Tests of Six Airfoils for Use on Small Wind Turbines," National Renewable Energy Laboratory, NREL/SR-500-34515, Oct. 2004.

[26]Uzol, O. and Camci, C., "The Effect of Sample Size, Turbulence Intensity and the Velocity Field on the Experimental Accuracy of Ensemble Averaged PIV Measurements," *4th International Symposium on Particle Image Velocimetry*, Sep. 2001.